

Atomic disorder and Berry phase driven anomalous Hall effect in a Co₂FeAl Heusler compoundGaurav K. Shukla,¹ Ajit K. Jena², Nisha Shahi¹, K. K. Dubey,¹ Indu Rajput,³ Sonali Baral³, Kavita Yadav⁴, K. Mukherjee⁴, Archana Lakhani³, Karel Carva,⁵ Seung-Cheol Lee,² Satadeep Bhattacharjee² and Sanjay Singh^{1,*}¹*School of Materials Science and Technology, Indian Institute of Technology (Banaras Hindu University), Varanasi 221005, India*²*Indo-Korea Science and Technology Center (IKST), Bangalore 560065, India*³*UGC-DAE Consortium for Scientific Research, Indore 452001, India*⁴*School of Basic Sciences, Indian Institute of Technology, Mandi 175005, India*⁵*Department of Condensed Matter Physics, Charles University, Ke Karlovu 5, CZ-12116 Praha, Czech Republic*

(Received 8 October 2021; revised 7 December 2021; accepted 4 January 2022; published 18 January 2022)

Co₂-based Heusler compounds are promising materials for spintronics applications due to their high Curie temperature, large spin polarization, large magnetization density, and exotic transport properties. In the present paper, we report the anomalous Hall effect (AHE) in a polycrystalline Co₂FeAl Heusler compound using combined experimental and theoretical studies. The Rietveld analysis of high-resolution synchrotron x-ray diffraction data reveals a large degree (~50%) of antisite disorder between Fe and Al atoms. The analysis of anomalous transport data provides the experimental anomalous Hall conductivity (AHC) about 227 S/cm at 2 K with an intrinsic contribution of 155 S/cm, which has nearly constant variation with temperature. The detailed scaling analysis of anomalous Hall resistivity suggests that the AHE in Co₂FeAl is governed by the Berry phase driven intrinsic mechanism. Our theoretical calculations reveal that the disorder present in the Co₂FeAl compound enhances the Berry curvature induced intrinsic AHC.

DOI: [10.1103/PhysRevB.105.035124](https://doi.org/10.1103/PhysRevB.105.035124)**I. INTRODUCTION**

The Hall effect is defined as the realization of a transverse electric field when a magnetic field is applied to a current-carrying conductor [1]. Ferromagnetic materials show an anomalous Hall effect (AHE) due to the interaction between spin-orbit coupling (SOC) and magnetization [1–4]. AHE finds renewed attention in condensed matter physics due to its huge application in magnetic sensors, random access memory, and spin logic devices [2,5,6]. Two possible mechanisms have been proposed to explain the origin of AHE: an extrinsic mechanism related to the scattering events, which includes skew scattering and side jumps, and another that is an intrinsic mechanism related to the band structure of the material [2,7,8]. The intrinsic mechanism was proposed by Karplus and Luttinger (KL theory of intrinsic mechanism), which is connected to the role of SOC in the electronic band structure of ferromagnetic materials and results in the anomalous velocity of electrons perpendicular to the electric field direction [2,9,10]. Later, KL theory was well understood in terms of the Berry phase and Berry curvature [11]. The Berry curvature is identical to a fictitious magnetic field in momentum space related to the geometrical phase of the electronic wave function [12]. The Berry curvature in momentum space introduces transverse momentum to the electrons and gives an intrinsic AHE [13,14].

The Berry curvature is highly sensitive to the electronic band structure of the material, and modulation in the band

structure can influence the Berry curvature and hence intrinsic anomalous Hall conductivity (AHC) [15]. The disorder may change the topology of the Fermi surface or position of the Fermi level or modify the local potential environment that breaks translational symmetry, inevitably modifying the band structure, which may reshape the AHE [15–19]. An increased AHC has been reported in a thin film of Co₂MnAl_{1-x}Si_x due to increased *L*₂₁ ordering within the lattice [18]. Recently, an enhancement in the AHC has been observed in Fe₂-based high Curie temperature Heusler compounds due to the increase in the crystal symmetry, when the system transforms from an inverse Heusler to *B*2 type (CsCl) structure [20].

Co₂-based full Heusler compounds got enormous attention for their half-metallic behavior, and 100% spin polarization around the Fermi level, which are the most prominent properties useful in spintronics devices and other memory-based applications [21–24]. Additionally, Co₂-based Heusler compounds are of current interest, because of their large AHE due to the large Berry curvature linked with their band structure [17,25–28]. Among Co₂-based Heusler compounds, Co₂FeAl is the most prominent candidate for data processing and storage-based applications due to its large Curie temperature (~810-900 K), high-spin polarization, low Gilbert damping factor, and ultrafast magnetization dynamics [29–33]. As the literature suggests that Co₂FeAl generally crystallizes into a *B*2-type [31,34–36] disordered structure, this compound therefore provides an opportunity for the investigation of the disorder effect on the Berry curvature and intrinsic AHC. Attempts to investigate anomalous transport in Co₂FeAl thin films report controversial results concerning the origin of AHE [34,35,37].

*ssingh.mst@iitbhu.ac.in

In the present paper, we studied AHE in a polycrystalline bulk Co_2FeAl Heusler compound. Synchrotron x-ray diffraction (SXR) data reveals a large degree of antisite disorder between the Fe and Al atoms. The experimental value of AHC was found to be about 227 S/cm at 2 K and 219 S/cm at 300 K with an intrinsic contribution of 155 S/cm. This intrinsic value of AHC is an order of magnitude larger than the theoretically predicted AHC for an ordered $L2_1$ phase of Co_2FeAl . Our theoretical calculations show that the antisite disorder present in Co_2FeAl enhances the Berry curvature induced intrinsic AHC.

II. METHODS

A polycrystalline Co_2FeAl Heusler compound was synthesized using a conventional arc melting technique using a stoichiometric amount of its high pure constituent elements. The compound was melted four times to ensure chemical homogeneity. A very small weight loss of 0.32% was noted after melting. Further, the ingot was sealed in a quartz ampoule under Ar atmosphere and then annealed at 800 °C for 12 h for better homogeneity. The energy dispersive x-ray (EDX) analysis reveals a composition ratio of 2:1:1 within the standard deviation (3%–5%) of the EDX measurement. A small piece was cut from the annealed ingot and crushed into powder for the SXR measurement. The SXR measurement was performed at PETRA-III, DESY for a structural analysis using a wavelength of 0.207 Å. Magnetic field-dependent magnetization measurements were carried out using the magnetic property measurement system (MPMS) from Quantum Design. A small polished rectangular piece was used for four-probe and five-probe magnetotransport measurements to obtain the longitudinal resistivity (ρ_{xx}) and the Hall resistivity (ρ_H), respectively. To obtain the actual ρ_H , raw Hall resistivity data (ρ_H^{raw}) were antisymmetrized by averaging the difference of ρ_H^{raw} at the positive and negative magnetic fields.

Electronic structure calculations were carried out using pseudopotential based density-functional theory and plane-wave basis sets as implemented in QUANTUM ESPRESSO (QE) [38], whereas the exchange-correlation potential is approximated through the Perdew-Burke-Ernzerhof generalized gradient approximation (PBE-GGA) functional [39]. Optimized norm-conserving Vanderbilt pseudopotentials [40] are used in the calculations and the kinetic energy cutoff for the plane wave is taken as 80 Ry. The electronic integration over the Brillouin zone is approximated by a Gaussian smearing of 0.01 Ry both for the self-consistent (SC) and non-self-consistent (NSC) calculations. The threshold for the SC energy calculations is taken as 10^{-8} Ry. The projections of Bloch wave functions are made into maximally localized Wannier functions. The WANNIER90 tool (implemented within QE) has been used to compute the Wannier interpolated bands and AHC [38,41,42]. SOC is introduced in all the calculations. A Monkhorst-Pack \mathbf{k} grid of $8 \times 8 \times 8$ is considered in the SC, NSC, and WANNIER90 calculations. The transition metal- d and Al- p orbitals are used as projections for the WANNIER90 calculations. The AHC calculation is carried out with a dense \mathbf{k} grid of $75 \times 75 \times 75$. Further, through the adaptive refinement technique, a fine mesh of $5 \times 5 \times 5$ is added around the points wherever the mode of the Berry curvature $[\Omega(\mathbf{k})]$

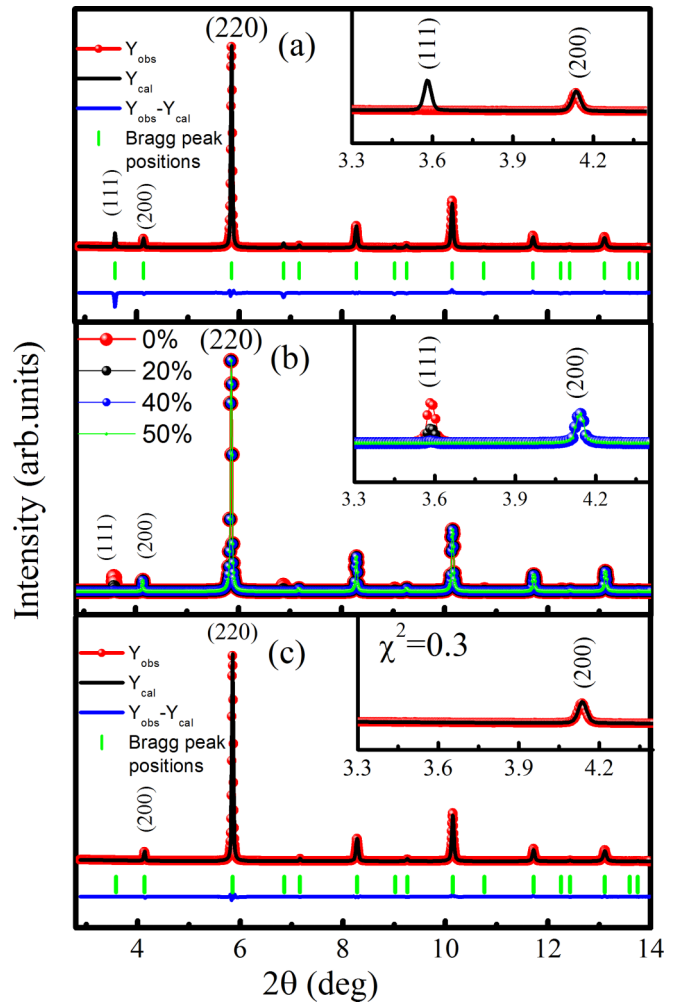


FIG. 1. (a) Rietveld refinement of the room-temperature (RT) synchrotron x-ray diffraction (SXR) pattern of Co_2FeAl considering an ordered $L2_1$ structure. (b) Simulated XRD patterns considering Fe and Al antisite disorder with indicated percentage. (c) Rietveld refinement of the RT SXR pattern of Co_2FeAl with 50% Fe and Al antisite disorder. The insets of the figures show an enlarged view around the (111) and (200) superlattice reflections.

exceeds 100 bohr². The calculations are carried out using an experimental lattice parameter.

III. RESULTS AND DISCUSSION

A. Structural analysis

The SXR pattern of the Co_2FeAl compound was collected at room temperature for a detailed analysis of crystal structure. In the first step, the Rietveld refinement of the SXR pattern was carried out using the $L2_1$ ordered cubic structure with space group $Fm\bar{3}m$. For the refinement, all the atoms were considered at special positions, i.e., Co at $8c$ (0.25, 0.25, 0.25), Fe at $4b$ (0.5, 0.5, 0.5), and Al at $4a$ (0, 0, 0) Wyckoff positions, respectively. The result of refinements is shown in Fig. 1(a).

We noticed the presence of (111) superlattice reflection in the calculated x-ray diffraction (XRD) pattern [black lines of

Fig. 1(a)], while this reflection is completely absent in the observed XRD pattern [red dots in Fig. 1(a)]. Interestingly, attempts to anneal the Co_2FeAl at different temperatures also could not show any remarkable difference in the XRD pattern in comparison to that observed in Fig. 1(a). It is important to mention here that atomic disorder is a common phenomenon in Heusler compounds [16,18,43]. The available literature also suggests that the Co_2FeAl crystallizes either in a $B2$ type structure, i.e., there is an antisite disorder between Fe and Al atoms (mutual swapping of the Fe and Al atomic position keeping the same stoichiometry) [31,34–36] or in a mixed phase of $L2_1$ and $B2$ structures [44]. However, the complete absence of a (111) peak in the SXRD pattern [inset of Fig. 1(a)] indicates the presence of antisite disorder in the present sample. So, in the next step we simulated the XRD pattern of Co_2FeAl considering the Fe-Al antisite disorder in such a way that the total number of Fe and Al atoms remains the same. For the XRD simulation, we used POWDERCELL software [45]. It is clear from Fig. 1(b) that the intensity of the (111) peak decreases with an increase in the amount of disorder and vanishes completely with about 50% antisite disorder between the Fe-Al atoms. Therefore, finally we performed the Rietveld refinement of the SXRD data assuming 50% antisite disorder between the Fe-Al atoms, which could fit the Bragg peaks very well [Fig. 1(c)] and confirm the phase purity (cubic) as well as the large antisite disorder ($B2$ type) in the sample. Moreover, the presence of a (200) Bragg peak primarily indicates the formation of an ordered Co sublattice and also precludes the possibility of A2 disorder (atomic disorder among all sites) in the sample. The intensity ratio of the superlattice reflection (200) and the fundamental reflection (220) (i.e., $\frac{I_{200}}{I_{220}}$) was found to be 0.048 and 0.046 from the experimental SXRD pattern and simulated XRD pattern, respectively, which are nearly the same, and further confirms the ordered Co sublattice in the present compound [34]. The refined unit cell parameter was found to be 5.73 Å, which is in good agreement with the literature [46,47].

B. Magnetization and resistivity

The magnetic moment obtained from the magnetic isotherms (Fig. 2) is about $5.74\mu_B/\text{f.u.}$ and $5.50\mu_B/\text{f.u.}$ at 2 and 300 K, respectively, which is close to the value reported in the literature [31,36,47–50]. The variation of ρ_{xx} as a function of temperature [Fig. 3(a)] depicts that ρ_{xx} increases with increasing temperature, indicating the metallic character of the compound. The residual resistance ratio [RRR = $\frac{\rho_{xx}(300\text{ K})}{\rho_{xx}(2\text{ K})}$] of about 1.25 is similar to the reported value for other Co_2 -based Heusler compounds [25,51,52].

C. Anomalous Hall

We carried out detailed magnetotransport measurements in a wide temperature range of 2–300 K to study the AHE in Co_2FeAl . The Hall resistivity (ρ_H) can be given by the equation $\rho_H = R_0H + R_sM$, where R_0 and R_s are the normal and anomalous Hall coefficients respectively. ρ_H vs H was measured at different temperatures up to a field of 7 T. From Fig. 3(b), it is evident that ρ_H steeply increases with fields up to 1 T, which can be observed due to AHE. However, under the

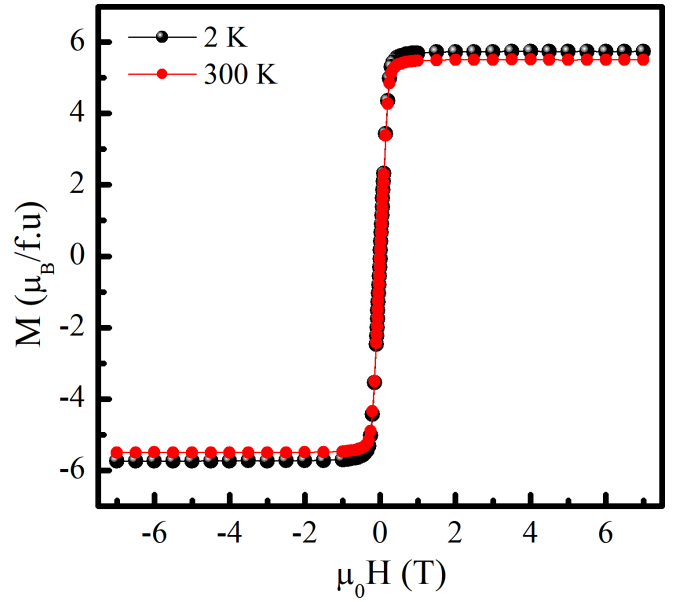


FIG. 2. Magnetic isotherms (M - H curves) recorded at 2 and 300 K.

application of higher fields (>1 T), a negative slope is noted due to the ordinary Hall effect. The normal Hall coefficient (R_0) was calculated from the slope of the high-field ρ_H curve. Figure 3(c) shows a temperature variation of R_0 . The negative value of R_0 indicates the electrons are the majority charge carriers. The inset of Fig. 3(c) shows the magnitude of carrier concentration (n) at different temperatures, calculated using the relation $R_0 = \frac{1}{ne}$, where n was found to be around 3×10^{21} at 300 K and the variation of n with temperature is slightly scattered. The anomalous Hall resistivity (ρ_{AH}) was calculated by extrapolating the high-field ρ_H curve on the y axis at zero field.

In order to elucidate the mechanism giving rise to AHE, we have plotted ρ_{AH} vs ρ_{xx} on a double logarithmic scale and fitting was employed to determine the exponent β using the relation $\rho_{AH} \propto \rho_{xx}^\beta$ [25] as shown in Fig. 3(d). If $\beta = 1$, the origin of AHE is assigned to the skew scattering, and if $\beta = 2$, the origin of AHE is due to intrinsic and side jump mechanisms [2,25]. We found the exponent $\beta = 1.69$, which indicates that the AHE in Co_2FeAl is dominated by the intrinsic and side jump mechanisms. The contribution of a side jump in AHC can be estimated using an expression $e^2/(ha)(\epsilon_{so}/E_F)$, where ϵ_{so} is the spin-orbit interaction and E_F is the Fermi energy [53,54]. The terms e , h , and a are the electronic charge, Planck constant, and lattice parameter, respectively. For most of the ferromagnetic metals ϵ_{so}/E_F is an order of 10^{-2} , and hence a very small contribution of AHC is expected due to a side jump in comparison to the intrinsic part of AHC. However, it is not possible to decouple the intrinsic and side jump mechanisms practically because both have similar dependencies on ρ_{xx} .

We have calculated the Hall conductivity using the tensor conversion $\sigma_H = \frac{\rho_H}{(\rho_H^2 + \rho_{xx}^2)}$ [43,55] as shown in the inset of Fig. 4(a). The AHC is calculated by averaging the extrapolated values of the high-field Hall conductivity curve at zero field of the positive and negative field directions. Temperature-dependent ρ_{AH} (black dots) and AHC (blue dots) are shown

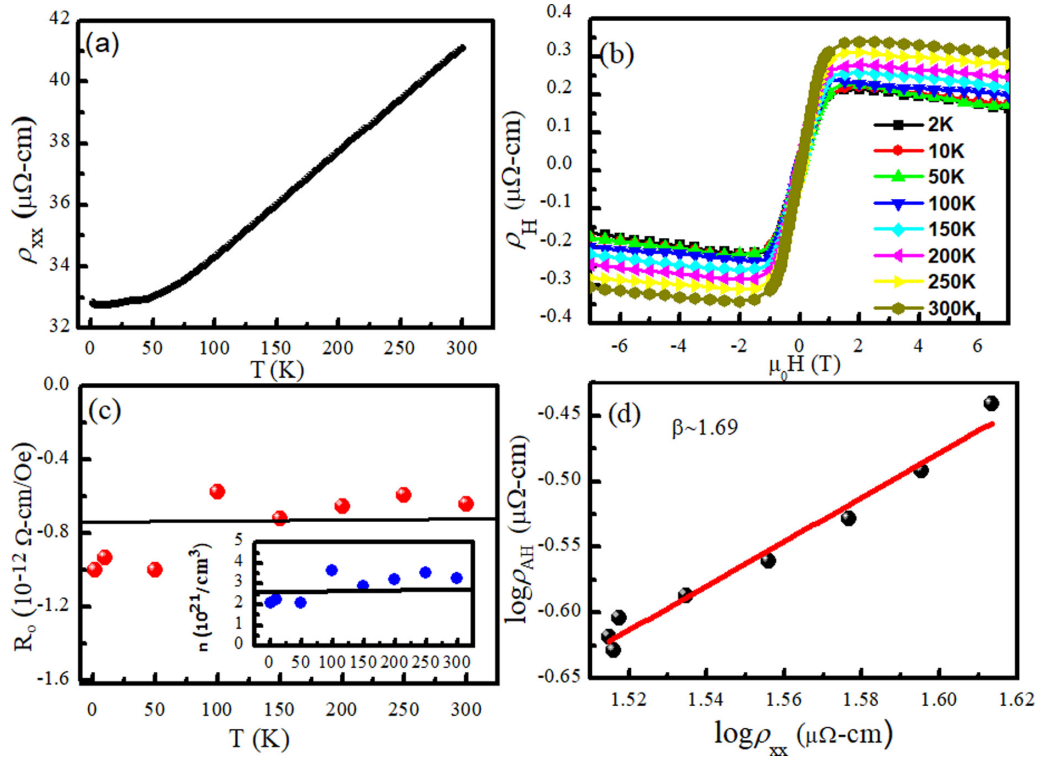


FIG. 3. (a) Temperature-dependent longitudinal resistivity ρ_{xx} . (b) Field-dependent Hall resistivity ρ_H at different temperatures. (c) Temperature-dependent normal Hall coefficient R_0 . The inset shows the temperature variation of carrier concentration n . (d) Experimental data (black dots) plotted between $\log \rho_{AH}$ and $\log \rho_{xx}$ and the fitted curve is shown in red color.

in Fig. 4(a). The value of AHC is found to be about 227 S/cm at 2 K and does not show an appreciable change at 300 K (219 S/cm). The variation of AHC is nearly temperature independent, suggesting that the origin of AHE is intrinsic [56,57].

To separate the extrinsic and intrinsic parts of AHE, we have plotted ρ_{AH} vs ρ_{xx} and fitted [Fig. 4(b)] according to the well-established equation for AHE, $\rho_{AH} = \alpha^{\text{skew}} \rho_{xx} + \sigma^{\text{int}} \rho_{xx}^2$, where α^{skew} and σ^{int} correspond to the skew scattering parameter and intrinsic AHC, respectively. σ^{int} was estimated as ~ 155 S/cm, which is about 70% of the total AHC at 2 K. Thus, in the present system, the intrinsic Berry phase driven KL contribution dominates along with finite skew scattering [2,56–58].

D. First principles calculation

After obtaining the experimental value of AHC, we have theoretically calculated AHC for Co_2FeAl by setting the magnetization direction along [001]. For Co_2 -based Heusler alloys the ground state energy in another magnetization direction such as [110] was found close to the [001] direction and the band structure was also found to be quite similar in both directions, therefore the average picture of AHC is expected to be close to the [001] direction [17,27,59,60]. The intrinsic AHC is proportional to the Brillouin zone (BZ) summation of the Berry curvature over all occupied states [61],

$$\sigma^{\alpha\beta} = \frac{e^2}{\hbar} \frac{1}{N} \sum_{\mathbf{k} \in (\text{BZ})} \Omega_{\gamma}(\mathbf{k}) f(\mathbf{k}), \quad (1)$$

where the indices α , β , and γ are the Cartesian coordinates. $f(\mathbf{k})$ stands for the Fermi distribution function, $\Omega_{\gamma}(\mathbf{k})$ denotes the γ component of the Berry curvature for the wave vector \mathbf{k} , and N is the number of electrons in the crystal. Further, the Berry curvature is related to the Berry connection $[A_n(\mathbf{k})]$ as

$$\Omega_n(\mathbf{k}) = \nabla_{\mathbf{k}} \times A_n(\mathbf{k}), \quad (2)$$

where n is the band index and $A_n(k)$ in terms of cell-periodic Bloch states $|u_{n\mathbf{k}}\rangle = e^{-ik \cdot r} |\psi_{n\mathbf{k}}\rangle$ is defined as $A_n(\mathbf{k}) = \langle u_{n\mathbf{k}} | i \nabla_{\mathbf{k}} | u_{n\mathbf{k}} \rangle$ [62]. In the first step of the AHC calculation, we considered the ordered $L2_1$ structure of Co_2FeAl , i.e., without any disorder. As discussed earlier, the intrinsic AHC of a system is strongly connected to its electronic band structure. In Fig. 5 (top), we have compared the full electronic band structure of $L2_1$ ordered Co_2FeAl with the Wannier interpolated one. The better interpolation suggests that it will provide WANNIER90 related properties accurately. The Wannier interpolation is a potential tool to calculate the momentum space integrals of rapidly varying functions [63]. Such integrals are involved in calculating the properties such as anomalous Hall conductivity, spin Hall conductivity, orbital magnetization, and optical properties [64]. The most popular technique to construct the Wannier functions is the maximally localized method [41] which is implemented in the WANNIER90 code [64]. The Wannier functions are generated using the unitary transformation of the Bloch wave function, so there is no loss of information during the generation. The main advantage of the Wannier interpolation over other approaches is that it allows for the most precise interpolation of band energies and

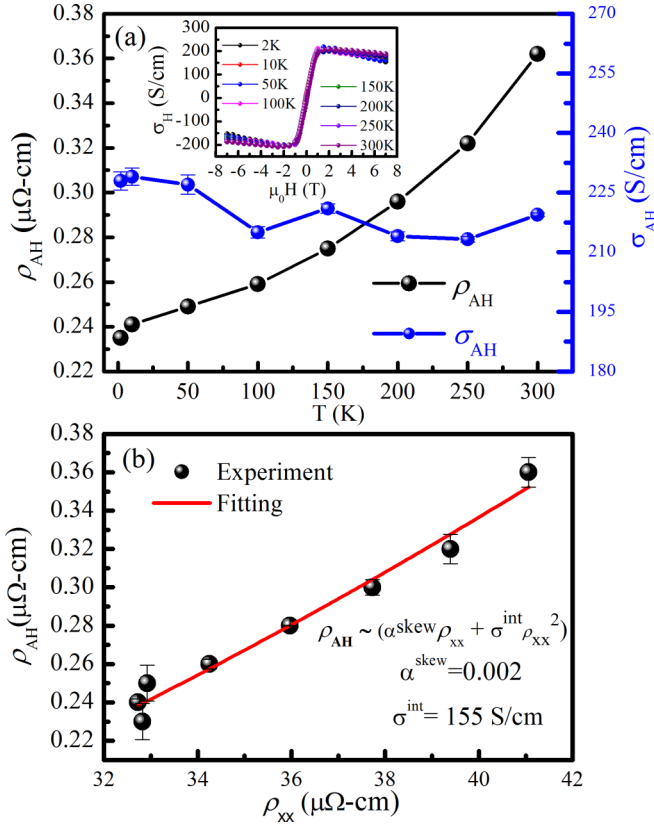


FIG. 4. (a) Anomalous Hall resistivity ρ_{AH} and anomalous Hall conductivity σ_{AH} as a function of temperature. The inset shows field-dependent Hall conductivity isotherms. (b) Experimental data (black dots) plotted as ρ_{AH} vs ρ_{xx} . The fitted curve is shown in red color.

matrix elements compared to other methods such as the tight binding approach because there is no limitation in terms of the size of the basis set [65].

By this method, we found the theoretical value of AHC (σ^{xy}) about ~ 42 S/cm, which is in good agreement with the literature [66]. Thus the theoretical AHC considering an ordered $L2_1$ structure is an order smaller than the experimental

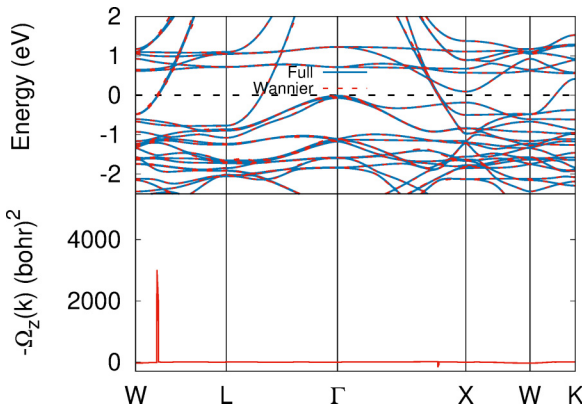


FIG. 5. Top: Comparison of Wannier interpolated band structure (red) with the full electronic band structure (blue) of Co_2FeAl . The Fermi energy is set to 0 eV. Bottom: Calculated Berry curvatures along the high-symmetry path.

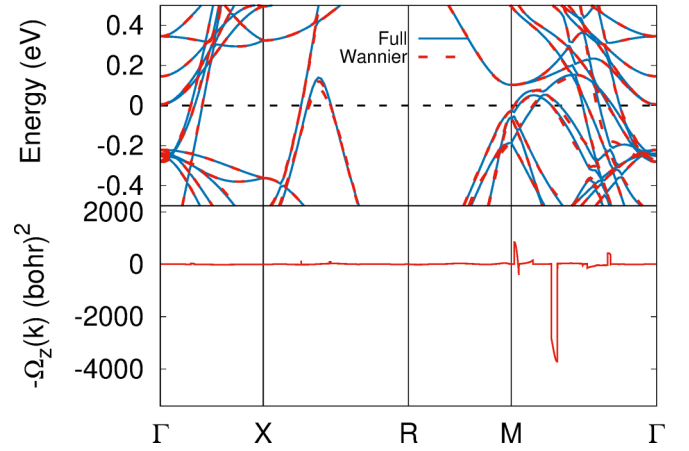


FIG. 6. Top: Comparison of Wannier interpolated band structure (red) with the full electronic band structure (blue) of disordered Co_2FeAl . The Fermi energy is set to 0 eV. Bottom: Calculated Berry curvatures along the high-symmetry path.

intrinsic AHC. Therefore, in the next step we incorporated 50% antisite disorder between the Al and Fe sites (as observed from the SXR analysis) in order to compute AHC for the disordered Co_2FeAl . In Fig. 6 (top), we have plotted the full electronic band structure of disordered Co_2FeAl with the Wannier interpolated band structure. The Berry curvature along the high-symmetry path of the disordered structure (space group $Pm\bar{3}m$) is depicted in Fig. 6 (bottom). The intrinsic AHC (σ^{xy}) for disordered Co_2FeAl calculated from the integration of Berry curvature turned out to be ~ 63 S/cm, which is interestingly larger than the ordered $L2_1$ structure. Thus, our theoretical calculations suggest that the disorder can modify the Berry curvature and result in an increased value of intrinsic AHC. Recently, it has been suggested in the literature that the presence of $B2$ disorder lowers the value of AHC in comparison to an ordered $L2_1$ structure [18,20]. Therefore, our combined experimental and theoretical results suggest that there is no straightforward rule that connects the Berry curvature to the disorder, but rather it depends on the disorder induced change in the electronic structure, which is different for different Heusler compounds as they have different numbers of electrons. If the effect of disorder is such that it brings the band crossings or avoided band crossing very close to the Fermi energy, then the value of Berry curvature will be large. We would also like to mention here that the experimentally found intrinsic AHC (155 S/cm) is larger than the theoretically predicted intrinsic AHC similar to other metallic compounds [17,56,66,67]. Hence, our results provide a platform for the systematic investigation of AHE in disordered Heusler compounds and related materials.

IV. CONCLUSIONS

In conclusion, we investigated the anomalous transport properties of a polycrystalline Co_2FeAl Heusler compound by experiment and theoretical calculations. SXR data reveal a large degree of Fe-Al antisite disorder. Experimental values of AHC were found to be 227 S/cm at 2 K and 219 S/cm at

300 K with an intrinsic AHC of 155 S/cm. Our experimental analysis shows that the AHE in Co_2FeAl is dominated by an intrinsic Berry phase mechanism. Our theoretical calculations suggest that the enhanced Berry curvature induced intrinsic AHC is linked with the antisite disorder present in the Co_2FeAl Heusler compound.

ACKNOWLEDGMENTS

We gratefully acknowledge UGC-DAE CSR for experimental support. S.S. thanks the Science and Engineering Research Board of India for financial support through the

award of Ramanujan Fellowship (Grant No. SB/S2/RJN-015/2017) and Early Career Research Award (Grant No. ECR/2017/003186), and UGC-DAE CSR, Indore for financial support through CRS Scheme. G.K.S. thanks the DST INSPIRE scheme for financial support. Portions of this research were conducted at the light source PETRA III of DESY, a member of the Helmholtz Association. Financial support from the Department of Science and Technology, Government of India within the framework of the India@DESY is gratefully acknowledged. We would like to thank the beamline scientist Dr. Martin Etter for his help in setting up the experiments.

-
- [1] N. Nagaosa, Anomalous Hall effect—A new perspective, *J. Phys. Soc. Jpn.* **75**, 042001 (2006).
- [2] N. Nagaosa, J. Sinova, S. Onoda, A. H. MacDonald, and N. P. Ong, Anomalous Hall effect, *Rev. Mod. Phys.* **82**, 1539 (2010).
- [3] Y. Tian, L. Ye, and X. Jin, Proper Scaling of the Anomalous Hall Effect, *Phys. Rev. Lett.* **103**, 087206 (2009).
- [4] D. Yue and X. Jin, Towards a better understanding of the anomalous Hall effect, *J. Phys. Soc. Jpn.* **86**, 011006 (2017).
- [5] S. Nakatsuji, N. Kiyohara, and T. Higo, Large anomalous Hall effect in a non-collinear antiferromagnet at room temperature, *Nature (London)* **527**, 212 (2015).
- [6] Q. Hao, W. Chen, S. Wang, and G. Xiao, Anomalous Hall effect and magnetic properties of $\text{Fe}_x\text{Pt}_{100-x}$ alloys with strong spin-orbit interaction, *J. Appl. Phys.* **122**, 033901 (2017).
- [7] J. Smit, The spontaneous Hall effect in ferromagnetics I, *Physica* **21**, 877 (1955).
- [8] J. Smit, The spontaneous Hall effect in ferromagnetics II, *Physica* **24**, 39 (1958).
- [9] R. Karplus and J. Luttinger, Hall effect in ferromagnetics, *Phys. Rev.* **95**, 1154 (1954).
- [10] G. Sundaram and Q. Niu, Wave-packet dynamics in slowly perturbed crystals: Gradient corrections and Berry-phase effects, *Phys. Rev. B* **59**, 14915 (1999).
- [11] D. Xiao, M.-C. Chang, and Q. Niu, Berry phase effects on electronic properties, *Rev. Mod. Phys.* **82**, 1959 (2010).
- [12] K. Manna, Y. Sun, L. Muechler, J. Kübler, and C. Felser, Heusler, Weyl and Berry, *Nat. Rev. Mater.* **3**, 244 (2018).
- [13] J. Ye, Y. B. Kim, A. J. Millis, B. I. Shraiman, P. Majumdar, and Z. Tešanović, Berry Phase Theory of the Anomalous Hall Effect: Application to Colossal Magnetoresistance Manganites, *Phys. Rev. Lett.* **83**, 3737 (1999).
- [14] Y. He, J. Moore, and C. M. Varma, Berry phase and anomalous Hall effect in a three-orbital tight-binding Hamiltonian, *Phys. Rev. B* **85**, 155106 (2012).
- [15] J. Shen, Q. Yao, Q. Zeng, H. Sun, X. Xi, G. Wu, W. Wang, B. Shen, Q. Liu, and E. Liu, Local Disorder-Induced Elevation of Intrinsic Anomalous Hall Conductance in an Electron-Doped Magnetic Weyl Semimetal, *Phys. Rev. Lett.* **125**, 086602 (2020).
- [16] E. Vilanova Vidal, H. Schneider, and G. Jakob, Influence of disorder on anomalous Hall effect for Heusler compounds, *Phys. Rev. B* **83**, 174410 (2011).
- [17] B. Ernst, R. Sahoo, Y. Sun, J. Nayak, L. Muechler, A. K. Nayak, N. Kumar, J. Gayles, A. Markou, G. H. Fecher, and C. Felser, Anomalous Hall effect and the role of Berry curvature in Co_2TiSn Heusler films, *Phys. Rev. B* **100**, 054445 (2019).
- [18] Y. Sakuraba, K. Hyodo, A. Sakuma, and S. Mitani, Giant anomalous nernst effect in the $\text{Co}_2\text{MnAl}_{1-x}\text{Si}_x$ Heusler alloy induced by Fermi level tuning and atomic ordering, *Phys. Rev. B* **101**, 134407 (2020).
- [19] J. Kudrnovský, V. Drchal, and I. Turek, Anomalous Hall effect in stoichiometric Heusler alloys with native disorder: A first-principles study, *Phys. Rev. B* **88**, 014422 (2013).
- [20] F. Mende, J. Noky, S. N. Guin, G. H. Fecher, K. Manna, P. Adler, W. Schnelle, Y. Sun, C. Fu, and C. Felser, Large anomalous Hall and Nernst effects in high Curie-temperature iron-based Heusler compounds, *Adv. Sci.* **8**, 2100782 (2021).
- [21] P. Brown, K.-U. Neumann, P. Webster, and K. Ziebeck, The magnetization distributions in some Heusler alloys proposed as half-metallic ferromagnets, *J. Phys.: Condens. Matter* **12**, 1827 (2000).
- [22] I. Galanakis, P. H. Dederichs, and N. Papanikolaou, Slater-Pauling behavior and origin of the half-metallicity of the full-Heusler alloys, *Phys. Rev. B* **66**, 174429 (2002).
- [23] J. Kübler, G. H. Fecher, and C. Felser, Understanding the trend in the Curie temperatures of Co_2 -based Heusler compounds: *Ab initio* calculations, *Phys. Rev. B* **76**, 024414 (2007).
- [24] H. C. Kandpal, G. H. Fecher, and C. Felser, Calculated electronic and magnetic properties of the half-metallic, transition metal based Heusler compounds, *J. Phys. D: Appl. Phys.* **40**, 1507 (2007).
- [25] S. Roy, R. Singha, A. Ghosh, A. Pariari, and P. Mandal, Anomalous Hall effect in the half-metallic Heusler compound Co_2TiX ($X = \text{Si}, \text{Ge}$), *Phys. Rev. B* **102**, 085147 (2020).
- [26] H. Reichlova, R. Schlitz, S. Beckert, P. Swekis, A. Markou, Y.-C. Chen, D. Kriegner, S. Fabretti, G. Hyeon Park, A. Niemann, S. Sudheendra, A. Thomas, K. Nielsch, C. Felser, and S. T. B. Goennenwein, Large anomalous Nernst effect in thin films of the Weyl semimetal Co_2MnGa , *Appl. Phys. Lett.* **113**, 212405 (2018).
- [27] P. Li, J. Koo, W. Ning, J. Li, L. Miao, L. Min, Y. Zhu, Y. Wang, N. Alem, C.-X. Liu, Z. Mao, and B. Yan, Giant room temperature anomalous Hall effect and tunable topology in a ferromagnetic topological semimetal Co_2MnAl , *Nat. Commun.* **11**, 3476 (2020).
- [28] I. Belopolski, K. Manna, D. S. Sanchez, G. Chang, B. Ernst, J. Yin, S. S. Zhang, T. Cochran, N. Shumiya, H. Zheng, B.

- Singh, G. Bian, D. Multer, M. Litskevich, X. Zhou, S.-M. Huang, B. Wang, T.-R. Chang, S.-Y. Xu, A. Bansil, C. Felser, H. Lin, and M. Z. Hasan, Discovery of topological Weyl fermion lines and drumhead surface states in a room temperature magnet, *Science* **365**, 1278 (2019); S. N. Guin, K. Manna, J. Noky, S. J. Watzman, C. Fu, N. Kumar, W. Schnelle, C. Shekhar, Y. Sun, J. Gooth, and C. Felser, Anomalous Nernst effect beyond the magnetization scaling relation in the ferromagnetic Heusler compound Co_2MnGa , *NPG Asia Mater.* **11**, 16 (2019).
- [29] S. Husain, N. Sisodia, A. K. Chaurasiya, A. Kumar, J. P. Singh, B. S. Yadav, S. Akansel, K. H. Chae, A. Barman, P. Muduli, P. Svedlindh, and S. Chaudhary, Observation of skyrmions at room temperature in Co_2FeAl Heusler alloy ultrathin film heterostructures, *Sci. Rep.* **9**, 1085 (2019).
- [30] X. Zhang, H. Xu, B. Lai, Q. Lu, X. Lu, Y. Chen, W. Niu, C. Gu, W. Liu, X. Wang, C. Liu, Y. Nie, L. He, and Y. Hu, Direct observation of high spin polarization in Co_2FeAl thin films, *Sci. Rep.* **8**, 8074 (2018).
- [31] S. Husain, S. Akansel, A. Kumar, P. Svedlindh, and S. Chaudhary, Growth of Co_2FeAl Heusler alloy thin films on Si (100) having very small Gilbert damping by ion beam sputtering, *Sci. Rep.* **6**, 28692 (2016).
- [32] R. S. Malik, E. K. Delczeg-Czirjak, R. Knut, D. Thonig, I. Vaskivskiy, D. Phuyal, R. Gupta, S. Jana, R. Stefanuik, Y. O. Kvashnin, S. Husain, A. Kumar, P. Svedlindh, J. Söderström, O. Eriksson, and O. Karis, Ultrafast magnetization dynamics in the half-metallic Heusler alloy Co_2FeAl , *Phys. Rev. B* **104**, L100408 (2021).
- [33] A. Kumar, F. Pan, S. Husain, S. Akansel, R. Brucas, L. Bergqvist, S. Chaudhary, and P. Svedlindh, Temperature-dependent Gilbert damping of Co_2FeAl thin films with different degree of atomic order, *Phys. Rev. B* **96**, 224425 (2017).
- [34] S. Husain, A. Kumar, S. Akansel, P. Svedlindh, and S. Chaudhary, Anomalous Hall effect in ion-beam sputtered Co_2FeAl full Heusler alloy thin films, *J. Magn. Magn. Mater.* **442**, 288 (2017).
- [35] X. Wang, Y. Li, Y. Du, X. Dai, G. Liu, E. Liu, Z. Liu, W. Wang, and G. Wu, Structural, magnetic and transport properties of Co_2FeAl Heusler films with varying thickness, *J. Magn. Magn. Mater.* **362**, 52 (2014).
- [36] M. Kogachi, N. Tadachi, and T. Nakanishi, Structural properties and magnetic behavior in $\text{CoFe}_{1-x}\text{Al}_x$ alloys, *Intermetallics* **14**, 742 (2006).
- [37] I.-M. Imort, P. Thomas, G. Reiss, and A. Thomas, Anomalous Hall effect in the Co-based Heusler compounds Co_2FeSi and Co_2FeAl , *J. Appl. Phys.* **111**, 07D313 (2012).
- [38] P. Giannozzi, S. Baroni, N. Bonini, M. Calandra, R. Car, C. Cavazzoni, D. Ceresoli, G. L. Chiarotti, M. Cococcioni, I. Dabo, A. D. Corso, S. de Gironcoli, S. Fabris, G. Fratesi, R. Gebauer, U. Gerstmann, C. Gougoussis, A. Kokalj, M. Lazzeri, L. Martin-Samos *et al.*, QUANTUM ESPRESSO: A modular and open-source software project for quantum simulations of materials, *J. Phys.: Condens. Matter* **21**, 395502 (2009).
- [39] J. P. Perdew, K. Burke, and M. Ernzerhof, Generalized Gradient Approximation Made Simple, *Phys. Rev. Lett.* **77**, 3865 (1996).
- [40] D. R. Hamann, Optimized norm-conserving Vanderbilt pseudopotentials, *Phys. Rev. B* **88**, 085117 (2013).
- [41] N. Marzari and D. Vanderbilt, Maximally localized generalized Wannier functions for composite energy bands, *Phys. Rev. B* **56**, 12847 (1997).
- [42] I. Souza, N. Marzari, and D. Vanderbilt, Maximally localized Wannier functions for entangled energy bands, *Phys. Rev. B* **65**, 035109 (2001).
- [43] B. K. Hazra, M. M. Raja, R. Rawat, A. Lakhani, S. Kaul, and S. Srinath, Effect of disorder on the anomalous Hall conductivity of Co_2FeSi thin films, *J. Magn. Magn. Mater.* **448**, 371 (2018).
- [44] R. Gupta, S. Husain, A. Kumar, R. Brucas, A. Rydberg, and P. Svedlindh, Co_2FeAl full Heusler compound based spintronic terahertz emitter, *Adv. Opt. Mater.* **9**, 2001987 (2021).
- [45] W. Kraus and G. Nolze, PowderCell—a program for the representation and manipulation of crystal structures and calculation of the resulting x-ray powder patterns, *J. Appl. Crystallogr.* **29**, 301 (1996).
- [46] G. Ortiz, M. Gabor, T. Petrisor, Jr, F. Boust, F. Issac, C. Tiusan, M. Hehn, and J. Bobo, Static and dynamic magnetic properties of epitaxial Co_2FeAl Heusler alloy thin films, *J. Appl. Phys.* **109**, 07D324 (2011).
- [47] S. Wurmehl, G. H. Fecher, K. Kroth, F. Kronast, H. A. Dürr, Y. Takeda, Y. Saitoh, K. Kobayashi, H.-J. Lin, G. Schönhense, and C. Felser, Electronic structure and spectroscopy of the quaternary Heusler alloy $\text{Co}_2\text{Cr}_{1-x}\text{Fe}_x\text{Al}$, *J. Phys. D: Appl. Phys.* **39**, 803 (2006).
- [48] V. Jain, V. Jain, V. Sudheesh, N. Lakshmi, and K. Venugopalan, Electronic structure and magnetic properties of disordered Co_2FeAl Heusler alloy, in *Solid State Physics: Proceedings of the 58th DAE Solid State Physics Symposium 2013*, edited by C. Murli, D. Bhattacharyya, and S. C. Gadkari, AIP Conf. Proc. Vol. 1591 (AIP, Melville, NY, 2014), pp. 1544–1545.
- [49] X. Zhang, W. Liu, Y. Yan, W. Niu, B. Lai, Y. Zhao, W. Wang, L. He, H. Meng, and Y. Xu, The atomic-scale magnetism of Co_2FeAl Heusler alloy epitaxial thin films, *Appl. Phys. Lett.* **113**, 212401 (2018).
- [50] A. Ahmad, S. Mitra, S. Srivastava, and A. Das, Size-dependent structural and magnetic properties of disordered Co_2FeAl Heusler alloy nanoparticles, *J. Magn. Magn. Mater.* **474**, 599 (2019).
- [51] A. Hirohata, M. Kikuchi, N. Tezuka, K. Inomata, J. Claydon, Y. Xu, and G. Van der Laan, Heusler alloy/semiconductor hybrid structures, *Curr. Opin. Solid State Mater. Sci.* **10**, 93 (2006).
- [52] A. Markou, D. Kriegner, J. Gayles, L. Zhang, Y.-C. Chen, B. Ernst, Y.-H. Lai, W. Schnelle, Y.-H. Chu, Y. Sun, and C. Felser, Thickness dependence of the anomalous Hall effect in thin films of the topological semimetal Co_2MnGa , *Phys. Rev. B* **100**, 054422 (2019).
- [53] P. Nozieres and C. Lewiner, A simple theory of the anomalous Hall effect in semiconductors, *J. Phys.* **34**, 901 (1973).
- [54] S. Onoda, N. Sugimoto, and N. Nagaosa, Intrinsic Versus Extrinsic Anomalous Hall Effect in Ferromagnets, *Phys. Rev. Lett.* **97**, 126602 (2006).
- [55] K. Manna, L. Muechler, T.-H. Kao, R. Stinshoff, Y. Zhang, J. Gooth, N. Kumar, G. Kreiner, K. Koepernik, R. Car, J. Kübler, G. H. Fecher, C. Shekhar, Y. Sun, and C. Felser, From Colossal to Zero: Controlling the Anomalous Hall Effect in Magnetic Heusler Compounds via Berry Curvature Design, *Phys. Rev. X* **8**, 041045 (2018).
- [56] Q. Wang, Y. Xu, R. Lou, Z. Liu, M. Li, Y. Huang, D. Shen, H. Weng, S. Wang, and H. Lei, Large intrinsic anomalous Hall

- effect in half-metallic ferromagnet $\text{Co}_3\text{Sn}_2\text{S}_2$ with magnetic Weyl fermions, *Nat. Commun.* **9**, 3681 (2018).
- [57] D. Liu, A. Liang, E. Liu, Q. Xu, Y. Li, C. Chen, D. Pei, W. Shi, S. Mo, P. Dudin, P. Dudin, T. Kim, C. Cacho, G. Li, Y. Sun, L. X. Yang, Z. K. Liu, S. S. P. Parkin, C. Felser, and Y. L. Chen, Magnetic Weyl semimetal phase in a kagomé crystal, *Science* **365**, 1282 (2019).
- [58] X. Chen, M. Wang, C. Gu, S. Wang, Y. Zhou, C. An, Y. Zhou, B. Zhang, C. Chen, Y. Yuan, M. Qi, L. Zhang, H. Zhou, J. Zhou, Y. Yao, and Z. Yang, Pressure-tunable large anomalous Hall effect of the ferromagnetic kagome-lattice Weyl semimetal $\text{Co}_3\text{Sn}_2\text{S}_2$, *Phys. Rev. B* **100**, 165145 (2019).
- [59] P. Chaudhary, K. K. Dubey, G. K. Shukla, S. Singh, S. Sadhukhan, S. Kanungo, A. K. Jena, S.-C. Lee, S. Bhattacharjee, J. Minár, and S. W. D'Souza, Role of chemical disorder in tuning the Weyl points in vanadium doped Co_2TiSn , *Phys. Rev. Mater.* **5**, 124201 (2021).
- [60] Z. Wang, M. G. Vergniory, S. Kushwaha, M. Hirschberger, E. V. Chulkov, A. Ernst, N. P. Ong, R. J. Cava, and B. A. Bernevig, Time-Reversal-Breaking Weyl Fermions in Magnetic Heusler Alloys, *Phys. Rev. Lett.* **117**, 236401 (2016).
- [61] J. Kübler and C. Felser, Berry curvature and the anomalous Hall effect in Heusler compounds, *Phys. Rev. B* **85**, 012405 (2012).
- [62] G. Pizzi, V. Vitale, R. Arita, S. Blügel, F. Freimuth, G. Géranton, M. Gibertini, D. Gresch, C. Johnson, T. Koretsune, J. Ibañez-Azpiroz, H. Lee, J.-M. Lihm, D. Marchand, A. Marrazzo, Y. Mokrousov, J. I. Mustafa, Y. Nohara, Y. Nomura, L. Paulatto *et al.*, Wannier90 as a community code: new features and applications, *J. Phys.: Condens. Matter* **32**, 165902 (2020).
- [63] S. S. Tsirkin, High performance Wannier interpolation of Berry curvature and related quantities with WannierBerri code, *npj Comput. Mater.* **7**, 33 (2021).
- [64] A. A. Mostofi, J. R. Yates, Y.-S. Lee, I. Souza, D. Vanderbilt, and N. Marzari, Wannier90: A tool for obtaining maximally-localised Wannier functions, *Comput. Phys. Commun.* **178**, 685 (2008).
- [65] S. Kundu, S. Bhattacharjee, S.-C. Lee, and M. Jain, Population analysis with Wannier orbitals, *J. Chem. Phys.* **154**, 104111 (2021).
- [66] H.-L. Huang, J.-C. Tung, and G.-Y. Guo, Anomalous Hall effect and current spin polarization in Co_2FeX Heusler compounds ($X = \text{Al, Ga, In, Si, Ge, and Sn}$): A systematic *ab initio* study, *Phys. Rev. B* **91**, 134409 (2015).
- [67] Y. Zhu, B. Singh, Y. Wang, C.-Y. Huang, W.-C. Chiu, B. Wang, D. Graf, Y. Zhang, H. Lin, J. Sun, A. Bansil, and Z. Mao, Exceptionally large anomalous Hall effect due to anticrossing of spin-split bands in the antiferromagnetic half-Heusler compound TbPtBi , *Phys. Rev. B* **101**, 161105(R) (2020).